Original Research

J. Minet*
S. Lambot
G. Delaide
J.A. Huisman
H. Vereecken
M. Vanclooster

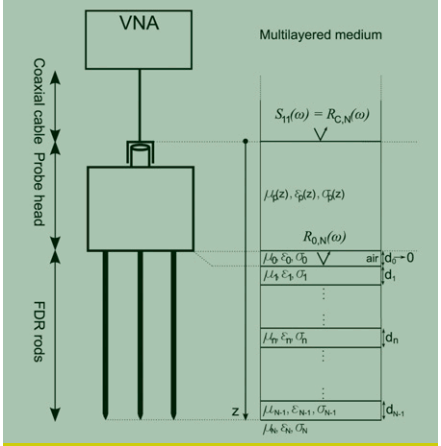

An electromagnetic model was developed for frequency domain reflectometry (FDR) based on the characterization of the FDR probe by transfer functions and on the decoupling of the probe signals from the ground signals. Inverse modeling of the FDR waveforms permits accurate retrieval of the frequency-dependent soil electrical properties.

J. Minet, S. Lambot, G. Delaide, and M. Vanclooster, Earth and Life Institute, Univ. Catholique de Louvain, Croix du Sud 2 BP 2, B-1348 Louvain-la-Neuve, Belgium; and S. Lambot, J.A. Huisman, and H. Vereecken, Agrosphere (ICG-4), Institute of Chemistry and Dynamics of the Geosphere, Forschungszentrum Jülich GmbH, D-52425 Jülich, Germany. *Corresponding author (julien.minet@uclouvain.be).

Vadose Zone J. 9:1063–1072
doi:10.2136/vzj2010.0004
Received 11 Jan. 2010.
Published online 20 Oct. 2010.
Freely available online through the author-supported open access option.

A Generalized Frequency Domain Reflectometry Modeling Technique for Soil Electrical Properties Determination

We have developed a generalized frequency domain reflectometry (FDR) technique for soil characterization that is based on an electromagnetic model decoupling the cable and probe head from the ground using frequency-dependent reflection and transmission transfer functions. The FDR model represents an exact solution of Maxwell's equations for wave propagation in one-dimensional multilayered media. The benefit of the decoupling is that the FDR probe can be fully described by its characteristic transfer functions, which are determined using only a few measurements. The soil properties are retrieved after removing the probe effects from the raw FDR data by iteratively inverting a global reflection coefficient. The proposed method was validated under laboratory conditions for measurements in water with different salt concentrations and sand with different water contents. For the salt water, inversions of the data led to dielectric permittivity and electrical conductivity values very close to the expected theoretical or measured values. In the frequency range for which the probe is efficient, a good agreement was obtained between measured, inverted and theoretically predicted signals. For the sand, results were consistent with the different water contents and also in close agreement with traditional time domain reflectometry measurements. The proposed method offers great promise for accurate soil electrical characterization because it inherently permits maximization of the information that can be retrieved from the FDR data and shows a high practicability.

Abbreviations: FDR, frequency domain reflectometry; TDR time domain reflectometry; VNA, vector network analyzer.

Time domain reflectometry (TDR) has become a standard in geophysical applications for measuring the soil dielectric permittivity and electrical conductivity. Since TDR for soil characterization was first developed by Topp et al. (1980, 2003) in the early 1980s, many applications and enhancements have been reported regarding (i) the development of the physical measurement system, e.g., the design of the TDR probe (Robinson et al., 2003) and the multiplexing of several probes (Heimovaara and Bouten, 1990), and (ii) the interpretation and modeling of the TDR waveform (Heimovaara, 1993; Noborio, 2001; Robinson et al., 2003). The calibration of petrophysical relationships that link the dielectric permittivity and the soil water content has also received specific attention (Topp et al., 1980; Ledieu et al., 1986; Sihvola and Kong, 1988; Yu et al., 1999).

Traditionally, dielectric permittivity is derived from the TDR signal by analysis of the travel time of the electromagnetic wave along the transmission line. Chung and Lin (2009) showed that different dielectric permittivity estimations can be obtained by comparing the methods that have been proposed to determine the reflection arrivals in the travel time analysis (e.g., the tangent method or the derivative method). Indeed, Hook and Livingston (1996) demonstrated that a dominant source of error in estimating soil water content using TDR was the uncertainty in determining the propagation travel time. High soil electrical conductivity in clay or saline soils can also significantly affect the propagation of the waveform and the determination of the travel time, leading to erroneous estimation of the real part of the dielectric permittivity if not taken into account (Pepin et al., 1995; Sun et al., 2000).

The soil electrical conductivity is usually retrieved from the TDR signal by depicting the reflection coefficient at long times and applying the Giese and Tiemann (1975) method; however, several researchers have pointed out the limitations of this method (Lin et al., 2008; Huisman et al., 2008) as well as the dielectric permittivity determination methods

cited above. In addition, these methods are not suited for determining the frequency dependence of the soil electrical properties.

To overcome these limitations, more advanced forward and inverse modeling methods, usually performed in the frequency domain, have shown promise (Heimovaara, 1994; Lin, 2003; Schaap et al., 2003; Huisman et al., 2004; Heimovaara et al., 2004; Mattei et al., 2005; Shuai et al., 2009). In addition, operating in the frequency domain permits increase of the bandwidth and, thereby, increases the information content in the data. As a result, frequency domain analysis offers more potential than the common time domain and travel time analysis methods for the determination of soil water content (Lin, 2003). Nevertheless, modeling of the FDR system could require numerous system calibrations with a high number of parameters to be determined (e.g., 40 as reported by Heimovaara et al., 2004) and the necessity of disconnecting the elements of the FDR system, as stated by Shuai et al. (2009). In addition, several assumptions about, e.g., the cable impedance and the characteristic probe impedance have to be made to resolve the FDR system. Given all of this, the practicability and accuracy of such methods remain questionable.

Electromagnetic wave generation can be performed using other wave generator devices than the commonly used and commercialized cable testers. In particular, FDR systems that have been conceived with a vector network analyzer (VNA) (Campbell, 1990; West et al., 2003; Huisman et al., 2004; Shuai et al., 2009) have shown an unprecedented precision and control of the input generated signal as well as on the reception and analysis of the returned waveform. In addition, the calibration of a VNA is well defined, constituting an international standard, and thereby ensures repeatability of the measurements. Finally, unified models and techniques have been developed for soil electromagnetic characterization based on the same VNA technology but using different sensors (e.g., ground penetrating radar [Lambot et al., 2004] and electromagnetic induction [Moghadas et al., 2010]) operating with different frequency ranges and measuring at different scales.

In this study, a generalized VNA-based FDR modeling approach was formulated and a practical probe calibration procedure was developed. The approach is based on an electromagnetic model decoupling the cable and probe head from the ground using frequency-dependent reflection and transmission transfer functions. The FDR model represents an exact solution of Maxwell's equations for wave propagation in one dimensional multilayered media and, in particular, in transmission lines. The FDR probe is fully described by its characteristic transfer functions, which are determined using three or more measurements for known model configurations. The soil properties are retrieved after removing the probe effects from the raw FDR data by iteratively inverting a multilayered global reflection coefficient. This approach is not limited to the VNA-based FDR setup used in this study and could be extended to the traditional TDR cable testers. To validate the method, we conducted laboratory experiments with measurements taken in salt water with increasing salt concentrations and sand with different moisture contents. The results were compared with theoretical values and traditional TDR estimates. The expected advantages of this approach compared with other existing methods are mainly the theoretical exactness of the model and the simple calibration procedure.

Materials and Methods

Theory

Electromagnetic Properties of Materials

The electromagnetic parameters governing wave propagation are the dielectric permittivity (ε), electrical conductivity (σ), and magnetic permeability (μ). The magnetic permeability of the major natural materials encountered in the environment is assumed to be equal to the magnetic permeability of free space, namely, $\mu_0 = 4\pi \times 10^{-7}$ H m^{-1}. Soil with magnetic materials (e.g., Fe oxides), however, may exhibit nonnegligible higher magnetic permeabilities (Robinson et al., 1994; van Dam et al., 2002; Stillman and Olhoeft, 2008; Mattei et al., 2008).

Due to relaxation phenomena, the soil electromagnetic properties present a frequency dependence, which is usually described with the extended Debye relaxation model (e.g., Heimovaara, 1994; Feng et al., 1999; Huisman et al., 2004). It is worth noting that this model assumes only one single relaxation phenomenon, while the soil is a mix of air, soil particles, and water and thus exhibits a complicated dielectric behavior due to the overlapping spectra of its different components (Logsdon, 2005). In the limited frequency range from 500 MHz to 3 GHz, however, it has been shown that the frequency dependence of the dielectric permittivity can be neglected for most soils (Zhou et al., 2001; Weerts et al., 2001; Huisman et al., 2002; Robinson et al., 2005). In this study, we assumed a constant dielectric permittivity in the frequency range 10 MHz to 1 GHz. The dielectric permittivity of sand can be assumed to be constant in that frequency range (Kelleners et al., 2005) and the dielectric permittivity of water or salt water decreases as a function of the frequency only above 2 GHz (Meissner and Wentz, 2004).

Nevertheless, the frequency dependence of the apparent electrical conductivity (which includes dielectric losses) in this frequency range can be significant, especially for high water contents. In a such limited frequency range, this dependence can be well accounted for using a linear model, thereby representing a local linear approximation of the full frequency-dependence function (Lambot et al., 2004):

$$\sigma(f) = \sigma_{f_{\min}} + s(f - f_{\min}) \quad [1]$$

where $\sigma_{f\min}$ is the apparent electrical conductivity at the minimum frequency of the frequency range ($f_{\min}$) and s the slope of the linear function $\sigma(f)$.

Modeling of the Frequency Domain Reflectometry System

An FDR (or TDR) system is typically constituted by an electromagnetic wave generator, a coaxial cable, and an FDR probe. The wave generator transmits an electromagnetic wave into the system and the FDR probe acts as a waveguide transmitting the wave into the medium in which the probe is inserted. The FDR rods thus emulate a coaxial medium where an alternating electric field oscillates between the central and the external rods, with the investigated medium acting as the insulating material of the coaxial line. Each sequential element of the FDR system is characterized by its internal electromagnetic properties, i.e., ε, σ, μ, and dimensions, determining its complex impedance. A change in these characteristic properties produces a partial reflection and transmission of the wave. The FDR system thereby constitutes a transmission line or a one-dimensional multilayered medium.

An FDR measurement using VNA technology is represented by the frequency-dependent scatter function $S_{11}(\omega)$, defined as the complex ratio between the reflected and incident waves:

$$S_{11} = \frac{B(\omega)}{A(\omega)} \quad [2]$$

where $B(\omega)$ and $A(\omega)$ are the reflected and incident waves, respectively, at the VNA calibration plane and ω is the angular frequency. The subscripts of $S_{11}(\omega)$ refer to the fact that the same port of the VNA (i.e., Port 1) is used for simultaneously transmitting (second subscript) and receiving (first subscript) the waves. Electromagnetic wave propagation through the FDR probe results from a combination of infinite multiple reflections and transmissions occurring at each change of impedance or interface.

In the time domain, using traditional TDR cable testers, the measured reflected wave $b(t)$ can be calculated by a convolution integral of the incident wave $a(t)$ and the system function $s(t)$ (Heimovaara, 1994):

$$b(t) = \int_{-\infty}^{+\infty} a(t-\tau)s(\tau)\mathrm{d}\tau \quad [3]$$

where τ is the integration variable. The measured reflected wave $b(t)$ in the time domain can then be transformed into the frequency domain wave $B(\omega)$ using a Fourier transform (Heimovaara, 1994).

The overall FDR system is shown in Fig. 1a and its corresponding representation in terms of a one-dimensional multilayered medium is shown in Fig. 1b. The variable $S_{11}(\omega)$ therefore represents a global reflection coefficient, measured at the calibration plane up to the end of the probe, formally referred to as $R_{C,N}(\omega)$, for fields incident from Layer C (the cable before the calibration plane) onto the interface with Layer N (the end of the rods). The probe head is defined here as the layered medium P, with unknown layers, situated between the calibration plane and the base of the FDR rods. To mathematically decouple the probe head from the FDR rods, a fictional air layer (Layer 0) is added in between, whose thickness (d_0) tends to zero. This layer therefore has no effect on the wave propagation. The FDR rods are then discretized into a number of layers representing a multilayered medium, with each soil layer being characterized by its own electromagnetic parameters and, by extension, its soil properties. For non-short-circuited probes, the end of the rods is modeled by an infinite half-space whose properties are defined such that they lead to a reflection coefficient $R_{N-1,N} = 1$. This can typically be emulated using relative dielectric permittivity $\varepsilon_r = 1$, $\sigma = 0$, and $\mu_r \to \infty$ for Layer N. The unknown layered medium P can be theoretically replaced by an equivalent medium with global reflection [$R_{C,0}(\omega)$ and $R_{0,C}(\omega)$] and transmission [$T_{C,0}(\omega)$ and $T_{0,C}(\omega)$] coefficients, defined as shown in Fig. 1c, which fully characterize the probe head. Indeed, the presence of the fictional air layer permits these global functions to be made independent from the soil properties. The scatter function $S_{11}(\omega)$ can then be derived as

$$S_{11}(\omega) = R_{C,N}(\omega) = R_{C,0}(\omega) + \frac{T_{C,0}(\omega)R_{0,N}(\omega)T_{0,C}(\omega)}{1 - R_{0,C}(\omega)R_{0,N}(\omega)} \quad [4]$$

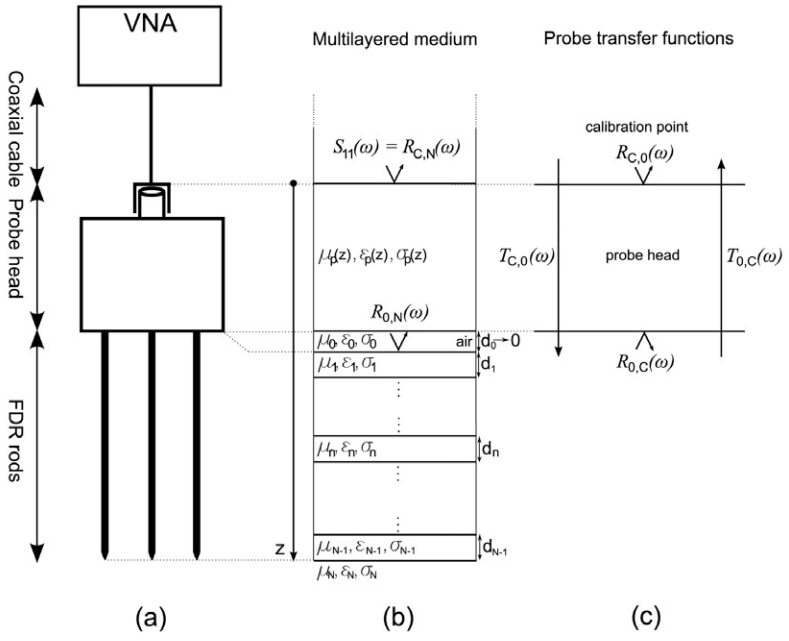

Fig. 1. Modeling of the frequency domain reflectometry (FDR) system by a one-dimensional multilayered medium: (a) schematic of the measurement system with vector network analyzer (VNA), (b) corresponding representation as a multilayered medium, where S_{11} is the scatter function, R are reflection coefficients, and ε is the dielectric permittivity, σ is the electrical conductivity, and μ is the magnetic permeability at depths d, and (c) probe reflection and transmission coefficients R and T characterizing the FDR probe head.

Defining $T(\omega) = T_{C,0}(\omega)T_{0,C}(\omega)$, the number of independent unknown characteristic probe head functions reduces to three, namely, $R_{C,0}(\omega)$, $R_{0,C}(\omega)$, and $T(\omega)$. It is worth noting that these characteristic probe transfer functions inherently contain the information about the probe characteristics such as, e.g., the probe impedance, which is integrated in the $T(\omega)$ and $R_{0,C}(\omega)$ transfer functions. Once these probe characteristic functions are known, the probe effects can be filtered out from the $S_{11}(\omega)$ measurements and the response of only the soil can be derived:

$$R_{0,N}(\omega) = \frac{S_{11}(\omega) - R_{C,0}(\omega)}{S_{11}(\omega)R_{0,C}(\omega) + T(\omega) - R_{C,0}(\omega)R_{0,C}(\omega)} \quad [5]$$

The three probe characteristic functions $R_{C,0}(\omega)$, $R_{0,C}(\omega)$, and $T(\omega)$ can be determined by solving a system of equations such as Eq. [4], for which at least three independent measurements of $S_{11}(\omega)$ should be performed and the corresponding $R_{0,N}(\omega)$ should be calculated. Practically, this can be realized using well-known model configurations such as shortcuts at different sections of the rods [assuming $R_{n,n+1}(\omega) = -1$ at the shortcut position] and a measurement with the probe in free space (air). To ensure independence of the calibrating equations across the whole frequency range, the system should ideally be overdetermined using more than three model configurations.

In the case of time domain measurements using classical TDR devices, the scatter function $S_{11}(\omega)$ measured by the VNA in Eq. [4] can be replaced by the reflected wave $B(\omega)$, that is, the Fourier transform of $b(t)$ measured by the TDR cable tester. In that case, the incident wave $A(\omega)$ is integrated into the probe characteristic functions $R_{C,0}(\omega)$ and $T(\omega)$; therefore, it is not necessary to know it. In a TDR system, the actual incident wave may differ from the one that is given by the TDR constructor because of distortions caused by internal electronics of the voltage generator and the transmission line (Mattei et al., 2005).

The global reflection coefficient from the FDR rods $[R_{0,N}(\omega)]$ can be recursively derived as (e.g., Feng et al., 1999; Heimovaara et al., 2004)

$$R_{n,N}(\omega) = \frac{R_{n,n+1}(\omega) + R_{n+1,N}(\omega)\exp\left[-2\gamma_{n+1}(\omega)d_{n+1}\right]}{1 + R_{n,n+1}(\omega)R_{n+1,N}(\omega)\exp\left[-2\gamma_{n+1}(\omega)d_{n+1}\right]} \quad [6]$$

where n refers to the layer (n = N − 1, N − 2, ..., 0), $\gamma_n(\omega)$ is the propagation constant, $R_{n,n+1}(\omega)$ is the local reflection coefficient for fields incident from the nth layer onto the interface with the layer $n + 1$, and d_n is the layer thickness. The recursion is initiated assuming $R_{N-1,N}(\omega) = 1$ for an open-ended probe (Feng et al., 1999; Schaap et al., 2003). The electromagnetic wave is assumed to propagate in the transverse electromagnetic mode, meaning that the electric and magnetic fields are transverse to the direction of the propagation of the wave. The propagation constant γ depends on the dielectric permittivity ε, electrical conductivity σ, and magnetic permeability μ of the medium. It is expressed as

$$\gamma(\omega) = \sqrt{-\omega^2\mu\left(\varepsilon - \frac{j\sigma}{\omega}\right)} \quad [7]$$

The propagation constant γ is a complex quantity, which can also be expressed as

$$\gamma = \alpha + j\beta \quad [8]$$

The real part, α, is the attenuation constant:

$$\alpha = \sqrt{\frac{\omega^2\mu\varepsilon}{2}\left(\sqrt{1+\tan^2\delta} - 1\right)} \quad [9]$$

and the imaginary part, β, is the phase constant:

$$\alpha = \sqrt{\frac{\omega^2\mu\varepsilon}{2}\left(\sqrt{1+\tan^2\delta} + 1\right)} \quad [10]$$

where

$$\tan\delta = \frac{\sigma}{\omega\varepsilon} \quad [11]$$

is defined as the loss tangent. The phase constant β determines wave propagation velocity (v) as

$$v = \frac{\omega}{\beta} = \frac{1}{\sqrt{(\mu\varepsilon/2)\left(\sqrt{1+\tan^2\delta} + 1\right)}} \quad [12]$$

It is worth noting that for nonmagnetic materials with a relatively low electrical conductivity and considering high frequencies, the wave propagation velocity can be approximated by

$$v \sim \frac{1}{\sqrt{\mu\varepsilon}} = \frac{c}{\sqrt{\varepsilon_r}} \quad [13]$$

where c is the wave velocity in free space and ε_r is the relative dielectric permittivity ($\varepsilon_r = \varepsilon/\varepsilon_0$ with ε_0 being the dielectric permittivity of free space). This assumption is commonly used when characterizing soil using classical TDR approaches. In our case, such an assumption was not applied.

The local reflection coefficient $R_{n,n+1}(\omega)$, resulting from the electromagnetic boundary conditions at an interface, is defined as

$$R_{n,n+1}(\omega) = \frac{\mu_{n+1}\gamma_n(\omega) - \mu_n\gamma_{n+1}(\omega)}{\mu_{n+1}\gamma_n(\omega) + \mu_n\gamma_{n+1}(\omega)} \quad [14]$$

Model Inversion

The unknown parameter vector **p** to be determined (containing the dielectric permittivity, frequency-dependent apparent electrical conductivity, and thickness of the investigated soil layers) is

retrieved by a full-waveform inversion procedure, which is applied to the probe-filtered FDR signal (see Eq. [5]). The inverse problem is formulated in the least squares sense and the objective function is defined as

$$\varphi(\mathbf{p}) = \left|\mathbf{R}_{0,N}{}^{*} - \mathbf{R}_{0,N}\right|^{T} \left|\mathbf{R}_{0,N}{}^{*} - \mathbf{R}_{0,N}\right| \quad [15]$$

where $\mathbf{R}_{0,N}{}^{*} = \mathbf{R}_{0,N}{}^{*}(\omega)$ and $\mathbf{R}_{0,N} = \mathbf{R}_{0,N}(\omega,\mathbf{p})$ are the vectors containing the observed and simulated global reflection coefficients, respectively, of the soil. Because these global reflection coefficients are complex vectors, the objective function is expressed by the amplitude of the difference of the filtered data in the complex plane.

Considering a multilayered soil sampled by the FDR probe, parameters for each soil layer can theoretically be retrieved by inversion, depending on the information content with respect to the number of parameters to optimize. Nevertheless, for thin layers compared with the signal wavelength and for small contrast between the layers, the information content in the waveform may be insufficient to distinguish the layers and to determine the layer properties, leading to nonuniqueness problems in the inversion, as was shown in Minet et al. (2010). Although the optimization problem is generally simple for a single soil layer, the topography of the objective function to minimize can be relatively complex when considering several soil layers, including multiple local minima. To properly solve such inverse problems, a global optimization procedure is required. Following the approach of Lambot et al. (2002), we used the global multilevel coordinate search algorithm (Huyer and Neumaier, 1999) combined sequentially with the classical Nelder–Mead simplex algorithm (Lagarias et al., 1998).

Water Content Determination

In this study, we used the model of Ledieu et al. (1986) to fit the inversely retrieved soil dielectric permittivity to the volumetric water content θ_v:

$$\theta = a\sqrt{\varepsilon_r} + b \quad [16]$$

where a and b are the optimized soil-specific parameters.

Laboratory Experiments Setup

The objective of the laboratory measurements was threefold: (i) to characterize the FDR probe transfer functions, (ii) to validate these transfer functions in a well-known medium, i.e., salt water, and (iii) to apply the inversion procedure to retrieve the electromagnetic properties of a wetted sand in which the probe was inserted.

We set up the FDR system using a VNA (ZVT8, Rohde & Schwarz, Münich, Germany) as transmitter and receiver, which we connected to a homemade FDR probe with high-quality N-type connectors and a 50-Ω impedance coaxial cable of 2.5-m length (Sucoflex 104PEA, Huber + Suhner AG, Herisau, Switzerland). The FDR probe was a 9.60-cm-length, three-rod stainless steel device held by an epoxy probe head and equipped with an N-type connector. The spacing between the two external rods was 28 mm and the diameter of the rods was 3 mm. The VNA was accurately calibrated with high precision [$S_{11}(\omega) < -90$ dB for a "Match" measurement] with a 50-Ω OSM (Open, Short, Match) series of a standard, N-type calibration kit (ZV-Z21, Rohde & Schwarz, Münich, Germany). The calibration of the VNA was made at the connector between the coaxial cable and the probe head, as illustrated in Fig. 1. It is worth noting that the calibration could also have been performed at Port 1 of the VNA. In that case, the probe transfer functions would have also accounted for the coaxial cable.

For the probe transfer functions determination, $S_{11}(\omega)$ measurements were first performed in different well-known media, namely, in air and with the FDR rods short-circuited at 16 different distances, accounting in total for 17 measurements, although three measurements are sufficient to determine the transfer functions. The probe length and the position of shortcuts along the probe were precisely measured to compute the theoretical global reflection coefficient in these media. Second, measurements in 10 saltwater solutions were made to validate the probe calibration and the inversion procedure. Last, we set up 10 different wetted sand media by mixing calculated volumes of dry sand and demineralized water to test the technique for the retrieval of the dielectric permittivities and frequency-dependent electrical conductivities. The same volume of water was added to the known volume of sand to obtain regularly increasing sand water content.

The frequency-dependent scatter function $S_{11}(\omega)$ was measured sequentially at 3996 stepped frequencies from 10 MHz to 8 GHz with a step of 2 MHz. Nevertheless, inversions of the measured signals were performed on a limited frequency range, namely, 10 to 1000 MHz, where the signal/noise ratio appeared to be optimal, especially due to the higher performances of the probe in that frequency range. It is worth mentioning that Lin (2003) suggested a similar optimal frequency range (500–1000 MHz).

For the measurements performed in the wetted sand, TDR measurements were also performed using a Tektronix 1502C metallic cable tester (Tektronix, Beaverton, OR) connected to a traditional TDR probe (95 mm long and 3-mm diameter with a 25-mm rod spacing). The dielectric permittivity was derived from the TDR waveforms using the WinTDR 6.0 software (Soil Physics Group, Utah State Univ., Logan).

Laboratory Experiments Results

Probe Transfer Functions Determination

The global reflection coefficients $R_{0,N}(\omega)$ corresponding to the 17 measurements (one air + 16 shortcuts) performed for the probe transfer functions determination were first calculated using Eq. [6]. The probe transfer functions were then retrieved by solving a system

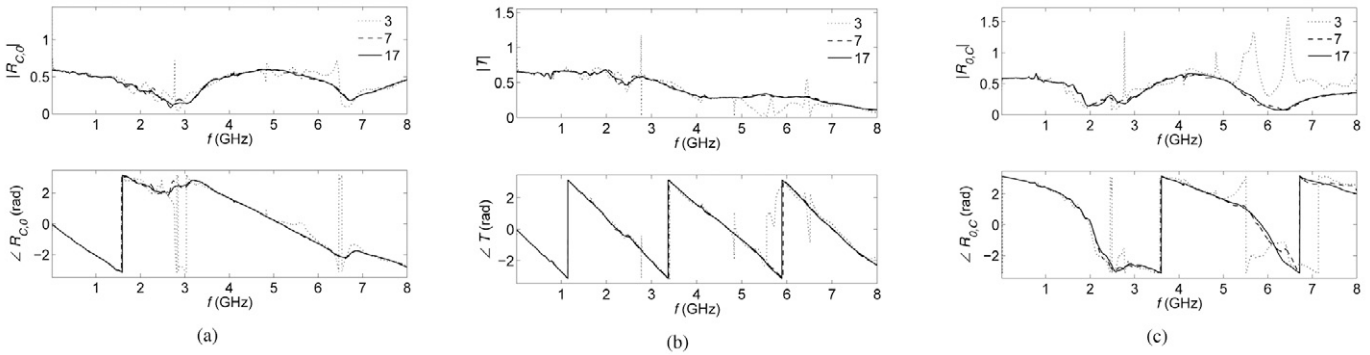

Fig. 2. Frequency domain reflectometry (FDR) probe transfer functions reflection coefficients (a) $R_{C,0}(\omega)$ and (c) $R_{0,C}(\omega)$ and transmission coefficients (b) $T(\omega)$ determined throughout the entire frequency range (f) from 10 MHz to 8 GHz, depicted in amplitude (upper graphs) and phase (lower graphs), for three different numbers of measurements (three, seven, and 17) used to solve the systems of equations.

of equations such as Eq. [4], assuming not only three model configurations but also more (seven and 17) to overdetermine the system.

Figure 2 shows the amplitude and phase of the FDR probe transfer functions $R_{C,0}(\omega)$, $T(\omega)$, and $R_{0,C}(\omega)$ determined across the full frequency range from 10 MHz to 8 GHz. The transfer functions determined with the minimal number of measurements (i.e., three) show very good results for frequencies in which the probe is the most efficient [low $R(\omega)$ and high $T(\omega)$ values in the lower frequency range], yet local errors appeared for some frequencies, especially in the higher frequency range where the signal/noise ratio became poor as a result of lower probe efficiency and sensitivity to measurement errors (e.g., in the measurement of the distance between the probe head and the shortcut). Overdetermining the system of equations using at least seven or more model configurations led to very similar values of the transfer functions across the whole frequency range, with smooth trends in terms of both amplitude and phase of the transfer functions, thereby denoting a good accuracy. For the analysis of the FDR data taken in salt water and wetted sand (see below), the transfer functions determined with the maximum number of measurements (i.e., 17) were used, but, as it can be observed in Fig. 2, seven measurements were already sufficient to obtain a high accuracy.

The analysis of these probe transfer functions permitted determining in which frequency range the probe is the most efficient. In particular, high $R_{C,0}(\omega)$ values (e.g., >0.5) indicate that, at these frequencies, most of the wave is reflected within the probe and is not transmitted to the ground. In contrast, high $T(\omega)$ values indicate that the probe is efficient at transmitting waves into the ground. In particular, we can see in Fig. 2b that the probe efficiency strongly decreased above 2 GHz because of the low $T(\omega)$ values. The $R_{0,C}(\omega)$ values can be analyzed similarly to $R_{C,0}(\omega)$, and low $R_{0,C}(\omega)$ were observed for the same frequency values as for $R_{C,0}(\omega)$, namely, around 3 and 6.5 GHz. Once they are characterized, these probe transfer functions can be used to filter out the raw measured data $S_{11}(\omega)$ from all the FDR probe head effects and obtain the global reflection coefficient of the FDR rod medium only [$R_{0,N}(\omega)$], namely, the soil. It is worth noting that in practice, only three reference measurements are required to accurately calibrate the probe, provided it is sufficiently efficient in the frequency range of concern.

Inversion of Frequency Domain Reflectometry Measurements in Salt Water

The validity of the probe calibration and of the inversion procedure was assessed by comparing the measured, theoretically predicted, and inverted (fitted) signals, as well as the theoretical or laboratory-measured and inverted parameters (i.e., ε_r, $\sigma_{f\min}$, and s) for the 10 measurements in salt water. The inversion was set in a large parameter space, namely, $2 < \varepsilon_r < 90$, $10^{-2} < \sigma_{f\min} < 10$ S m^{-1} and $10^{-11} < s < 10^{-7}$ s S m^{-1}, and more than 5400 iterations were performed. Salt concentrations were regularly increased from 0.154 to 1.540 g L^{-1} by adding precise quantities of NaCl into demineralized water. The solution electrical conductivity, as well as the solution temperature, was measured by a WTW LF318 (WTW, Weilheim, Germany) conductivity meter. Bulk electrical conductivity measurements were then temperature corrected to obtain the actual electrical conductivity at the solution temperature. According to the data sheet of the conductivity meter, measurement errors are 10^{-4} and 10^{-3} S m^{-1} for conductivities smaller and larger than 0.2 S m^{-1}, respectively.

Figure 3 shows the measured, predicted, and inverted scatter functions $S_{11}(\omega)$ arising from the whole FDR probe, including the probe head, for a measurement in salt water with the lowest salt concentration (0.154 g L^{-1}) depicted in the frequency domain in amplitude and phase (Fig. 3a) and in the time domain (Fig. 3b). Under laboratory conditions, the measured scatter functions showed a good reproducibility, with identical measured signals with repeated measurements. The inverted parameters were used to compute the inverted global reflection coefficient, which was then translated backward into the inverted scatter function $S_{11}(\omega)$ using Eq. [4]. The predicted scatter function

was computed using the electromagnetic model and theoretical permittivity and conductivity values estimated by a formulation of the Debye model for salt water from Meissner and Wentz (2004) using the measured bulk electrical conductivity and temperature. This accurate model accounts for the frequency and temperature dependence of the electrical parameters, but it is restricted to salt water only. Measurement errors of the bulk electrical conductivity ($\Delta\sigma$ = 0.0001 S m^{-1}) and of the solution temperature (ΔT = 0.1°C) do not have a visible impact on the predicted signal when propagating the errors to the predicted scatter function $S_{11}(\omega)$ (RMSE of 0.00110 in terms of amplitude of the scatter function in the frequency domain).

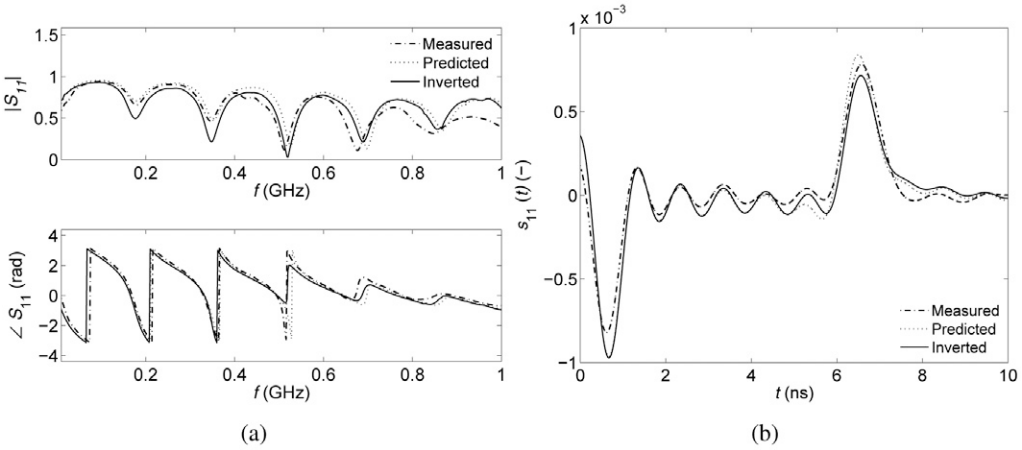

Fig. 3. Measured, predicted, and inverted scatter functions $S_{11}(\omega)$ depicted in the (a) frequency (f) and (b) time (t) domains for water with a salt concentration of 0.154 g L^{-1}.

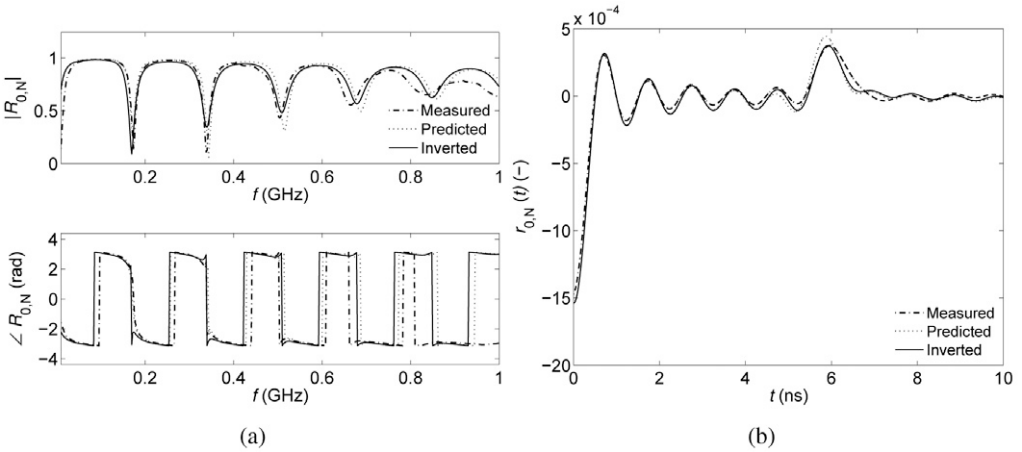

Fig. 4. Measured, predicted, and inverted global reflection coefficients $R_{0,N}(\omega)$ depicted in the (a) frequency (f) and (b) time (t) domains for water with a salt concentration of 0.154 g L^{-1}.

In the frequency domain, some discrepancies were observed between the measured and inverted or predicted signals, both in amplitude and phase, especially with increasing frequency. These discrepancies may be attributed to a lower signal/noise ratio as a result of the stronger attenuation of the waves due to increasing relaxation phenomena with increasing frequency. In the time domain, the reflection at the beginning of the FDR rods was observed around 1 ns and the final reflection from the end of the probe after 6 ns. Arrival times of the reflection were identical between the measured, inverted, and predicted signals, whereas there was a poorer agreement between the amplitudes of the reflection peaks. For the inverted signal, this indicates a high sensitivity of the model to the dielectric permittivity, which mainly governs the propagation time, rather than the electrical conductivity.

Figure 4 shows the corresponding measured, predicted, and inverted global transfer coefficients $R_{0,N}(\omega)$ depicted in the frequency domain in amplitude and phase (Fig. 4a) and in the time domain (Fig. 4b) for the same saltwater medium as shown in Fig. 3. In the frequency domain, discrepancies between the measured and inverted or predicted signals are smaller than in Fig. 3a, although increasing errors with frequency can still be observed. For low frequencies (e.g., <600 MHz), the inverted signal fits the measured signal remarkably well. In the time domain, the same agreement between the measured and inverted, as well as the predicted signals also can be observed. It is worth noting that the signal appears to be better modeled when expressed in terms of $R_{0,N}$ because it is referenced with respect to the fictional air layer, resulting in a larger contrast at the beginning of the FDR rods. In particular, the reflection of the end of the probe is relatively higher for the signal expressed in terms of S_{11} when comparing with $R_{0,N}$ because $R_{0,N}$ is computed assuming that less signal is transmitted in the FDR rods.

Corresponding with the case depicted in Fig. 4, the inverted parameters that were retrieved are ε_r = 84.4, σ_{10MHz} = 0.0210 S m^{-1} and $s = 10^{-9.55}$ s S m^{-1}. The relative dielectric permittivity ε_r at the solution temperature (13.5°C) is expected to range from 82.2 to 82.6 in the limited frequency range of 10 to 1000 MHz (Meissner and Wentz, 2004), which is close to the inverted dielectric permittivity value. The slight overestimation of the water dielectric permittivity is expected to have come from the fact that,

during the measurements with the probe in the water, some water wetted the inside of the probe head through the rods. The measured solution bulk conductivity with the conductivity meter was, for that case, 0.0242 ± 0.0001 S m^{-1}.

Figure 5 compares the measured and inverted electrical conductivity values for the 10 different saltwater solutions. Inverted frequency-dependent electrical conductivities were chosen at the minimum frequency of 10 MHz. There is a very good agreement between these two variables, with r^2 = 0.997. Inverted values were slightly underestimated compared with the measured electrical conductivities, but inverted values can be higher considering higher frequencies. The relation between the mass of added salt in the solution and the measured electrical conductivity appears to be linear in this range of salinity (not shown) and also well determined, with r^2 = 0.999. Inverted dielectric permittivity values were very similar between the 10 saltwater solutions, ranging from 84.39 to 84.69. The good agreement of the measured or theoretical and inverted parameters, as well as the small discrepancies between theoretically predicted, inverted, and measured signals, demonstrate the accuracy of the electromagnetic model and probe transfer functions determination with respect to real measurements, as well as that the inverse problem was well posed.

Determination of the Sand Water Content

The measured FDR signals from the 10 wetted sand media were filtered for the probe effects using Eq. [5] and then inverted in the limited frequency range of 10 to 1000 MHz to retrieve the soil dielectric permittivity and the frequency-dependent apparent electrical conductivity. The parameter space for the inversion was set as follows: $2 < \varepsilon_r < 90$, $10^{-4} < \sigma_{fmin} < 10^{-1}$ S m^{-1}, and $10^{-12} < s < 10^{-5}$ s S m^{-1}. The media were assumed to be homogeneous in the electromagnetic model ($N = 2$ in Fig. 1). Subsequent to the FDR measurements, volumetric samples of the wetted sand were collected to determine the actual water content, using the oven-drying method at 105°C for at least 48 h.

Figure 6 shows the relative dielectric permittivity estimated from TDR measurements and FDR inversions as a function of the sand water content measured by volumetric sampling. The model of Ledieu et al. (1986) (Eq. [16]) linking the volumetric water content and the dielectric permittivity was fitted on both TDR and FDR data. The RMSE of the fits and the r^2 between $\sqrt{\varepsilon_r}$ and θ_v are shown in Table 1.

Both TDR and FDR relationships are very good, with r^2 close to 1 and RMSE close to 0.5 in terms of dielectric permittivity, corresponding to an error of <1% in terms of θ_v. The differences between FDR and TDR estimates may originate from the uncertainties in the volumetric sampling and from the different locations where the FDR and TDR probes were inserted, given the inherent heterogeneities in the sand water content and density.

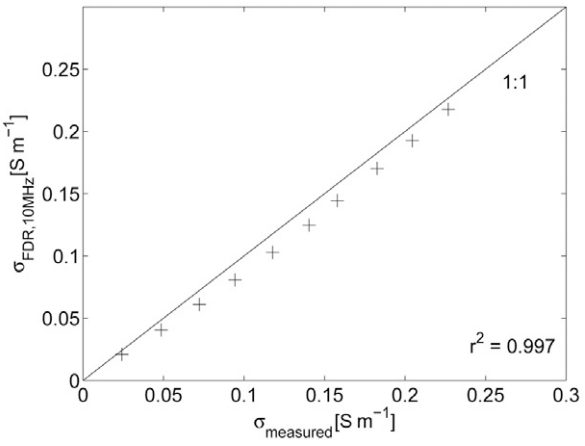

Fig. 5. Inverted electrical conductivity (σ) at the minimal frequency (10 MHz) from frequency domain reflectometry (FDR) measurements as a function of the measured σ in the 10 different saltwater solutions.

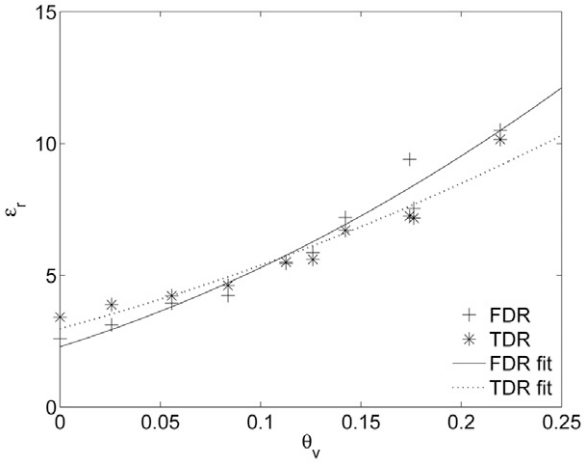

Fig. 6. Relative dielectric permittivity (ε_r) estimated from time domain reflectometry (TDR) measurements and frequency domain reflectometry (FDR) inversions as a function of the sand water content (θ_v) measured by volumetric sampling. The model of Ledieu et al. (1986) was fitted over the TDR and FDR data.

Table 1. Root mean square error of the fits according to the model of Ledieu et al. (1986) and coefficient of determination (r^2) between the square root of the relative dielectric permittivity and the volumetric water contents for time domain reflectometry (TDR) and frequency domain reflectometry (FDR) measurements.

Method	RMSE	r^2
TDR	0.461	0.948
FDR	0.514	0.965

Figure 7 shows the frequency-dependent electrical conductivity, $\sigma(f)$ inverted from FDR signals for the 10 different sand water contents (depicted from water contents [WC] 1 to 10 in Fig. 7b) as a function of the frequency range in which the data were inverted. Frequency-dependent electrical conductivity determined from an

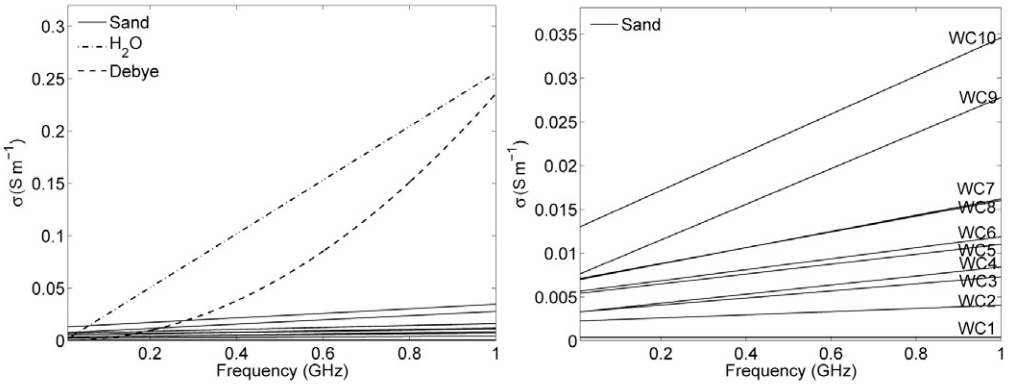

Fig. 7. Frequency-dependent, apparent electrical conductivity (σ) retrieved from frequency domain reflectometry (FDR) inversions for sand media at 10 different water contents (WC) and for demineralized water depicted with theoretical values from the model of Debye; (b) enlargement of the electrical conductivity of the sand media.

FDR measurement in demineralized water and the theoretical Debye model for pure water according to the parameterization of Meissner and Wentz (2004) are shown for comparison purposes.

The slopes of the linear frequency dependence for the different wetted sands are different, ranging from $10^{-25.3}$ to $10^{-10.6}$ s S m^{-1}, for the lowest and highest sand water contents, respectively. Not surprisingly, the apparent electrical conductivity increased with the sand water content, tending to the slope of demineralized water ($s = 10^{-9.59}$ s S m^{-1}). Nevertheless, the apparent frequency-dependent electrical conductivity of the most wetted sand remained far from the frequency-dependent electrical conductivity of water because of the composition of wetted sand, which is a mix of air, water, and soil particles. The assumption of linearity of the frequency dependence appears to be quite acceptable for pure water, with a line approaching the curved Debye model. It is worth noting that, at the lowest and highest frequencies, the inverted frequency-dependent electrical conductivities of demineralized water measurement correspond to the values calculated with the theoretical Debye model.

Conclusions

We developed a new FDR technique based on an electromagnetic model decoupling the FDR probe head from the measured medium using three frequency-dependent transfer functions. At least three laboratory measurements in perfectly known media and modeling of the global reflection coefficients in these configurations can be used to fully determine the probe transfer functions, owing to the decoupling of the FDR probe and the accurate electromagnetic modeling. The technique was validated with measurements in saltwater media. Measured, inverted, and theoretically predicted signals in the frequency range in which the probe is efficient were in close agreement, thereby demonstrating the accuracy of the whole forward model and that inverse problems were well posed. A very good agreement was also observed when comparing measured or theoretical and inverted parameters, i.e., the dielectric permittivities and electrical conductivities. Measurements in 10 different wetted sands were then conducted and the dielectric permittivities retrieved from FDR inversions were close to the values derived from classical TDR measurements and in a good agreement with volumetric water contents, with r^2 between $\sqrt{\varepsilon_r}$ and θ_v of 0.948 and 0.965 for the TDR and FDR methods, respectively. Moreover, the frequency-dependent electrical conductivity could also be determined. The proposed method appears promising for readily calibration of the FDR probe, for assessing the frequency dependence of the electrical properties and for inverting waveforms coming from multilayered media.

Acknowledgments

This work was supported by the Belgian Science Policy Office in the frame of the Stereo II program- project SR/00/100 (HYDRASENS), the DIGISOIL project financed by the European Commission under the 7th Framework Program for Research and Technological Development, Area "Environment", Activity 6.3 "Environmental Technologies", and the Fonds de la Recherche Scientifique (FNRS, Belgium). The authors are grateful to David Robinson and two anonymous reviewers for their constructive comments.

References

Campbell, J.E. 1990. Dielectric properties and influence of conductivity in soils at one to fifty megahertz. Soil Sci. Soc. Am. J. 54:332–341.

Chung, C.C., and C.P. Lin. 2009. Apparent dielectric constant and effective frequency of TDR measurements: Influencing factors and comparison. Vadose Zone J. 8:548–556.

Feng, W., C.P. Lin, R.J. Deschamps, and V.P. Drnevich. 1999. Theoretical model of a multisection time domain reflectometry measurement system. Water Resour. Res. 35:2321–2331.

Giese, K., and R. Tiemann. 1975. Determination of the complex permittivity from thin-sample time domain reflectometry: Improved analysis of the step response waveform. Adv. Mol. Relax. Interact. Processes 7:45–59.

Heimovaara, T.J. 1993. Time domain reflectometry in soil science: Theoretical backgrounds, measurements and models. Ph.D. diss. Amsterdam Univ., Amsterdam.

Heimovaara, T.J. 1994. Frequency domain analysis of time domain reflectometry waveforms: 1. Measurements of the complex dielectric permittivity of soils. Water Resour. Res. 30:189–199.

Heimovaara, T.J., and W. Bouten. 1990. A computer-controlled 36-channel time domain reflectometry system for monitoring soil water contents. Water Resour. Res. 26:2311–2316.

Heimovaara, T.J., J. Huisman, J.A. Vrugt, and W. Bouten. 2004. Obtaining the spatial distribution of water content along a TDR probe using the SCEM-UA Bayesian inverse modeling scheme. Vadose Zone J. 3:1128–1145.

Hook, W.R., and N.J. Livingston. 1996. Errors in converting time domain reflectometry measurements of propagation velocity to estimates of soil water content. Soil Sci. Soc. Am. J. 60:35–41.

Huisman, J.A., W. Bouten, and J.A. Vrugt. 2004. Accuracy of frequency domain analysis scenarios for the determination of complex dielectric permittivity. Water Resour. Res. 40:W02401, doi:10.1029/2002WR001601.

Huisman, J.A., C.P. Lin, L. Weihermüller, and H. Vereecken. 2008. Accuracy of bulk electrical conductivity measurements with time domain reflectometry. Vadose Zone J. 7:426–433.

Huisman, J.A., A.H. Weerts, T.J. Heimovaara, and W. Bouten. 2002. Comparison of travel time analysis and inverse modeling for soil water content determination with time domain reflectometry. Water Resour. Res. 38(6):1077, doi:10.1029/2001WR000259.

Huyer, W., and A. Neumaier. 1999. Global optimization by multilevel coordinate search. J. Global Optim. 14:331–355.

Kelleners, T.J., D.A. Robinson, P.J. Shouse, J.E. Ayars, and T.H. Skaggs. 2005. Frequency dependence of the complex permittivity and its impact on dielectric sensor calibration in soils. Soil Sci. Soc. Am. J. 69:67–76.

Lagarias, J.C., J.A. Reeds, M.H. Wright, and P.E. Wright. 1998. Convergence properties of the Nelder–Mead simplex method in low dimensions. SIAM J. Optim. 9:112–147.

Lambot, S., M. Javaux, F. Hupet, and M. Vanclooster. 2002. A global multilevel coordinate search procedure for estimating the unsaturated soil hydraulic properties. Water Resour. Res. 38:1224.

Lambot, S., E.C. Slob, I. van den Bosch, B. Stockbroeckx, and M. Vanclooster. 2004. Modeling of ground penetrating radar for accurate characterization of subsurface electric properties. IEEE Trans. Geosci. Remote Sensing 42:2555–2568.

Ledieu, J., P. De Ridder, P. De Clercq, and S. Dautrebande. 1986. A method of measuring soil moisture by time domain reflectometry. J. Hydrol. 88:319–328.

Lin, C.-P. 2003. Frequency domain versus travel time analyses of TDR waveforms for soil moisture measurements. Soil Sci. Soc. Am. J. 67:720–729.

Lin, C.-P., C.-C. Chung, J.A. Huisman, and S.-H. Tang. 2008. Clarification and calibration of reflection coefficient for electrical conductivity measurement by time domain reflectometry. Soil Sci. Soc. Am. J. 72:1033–1040.

Logsdon, S.D. 2005. Soil dielectric spectra from vector network analyzer data. Soil Sci. Soc. Am. J. 69:983–989.

Mattei, E., A. De Santis, A. Di Matteo, E. Pettinelli, and G. Vannaroni. 2005. Time domain reflectometry of glass beads/magnetite mixtures: A time and frequency domain study. Appl. Phys. Lett. 86(22):224102, doi:10.1063/1.1935029.

Mattei, E., A. De Santis, A. Di Matteo, E. Pettinelli, and G. Vannaroni. 2008. Electromagnetic parameters of dielectric and magnetic mixtures evaluated by time-domain reflectometry. IEEE Geosci. Remote Sens. Lett. 5:730–734.

Meissner, T., and F.J. Wentz. 2004. The complex dielectric constant of pure and sea water from microwave satellite observations. IEEE Trans. Geosci. Remote Sensing 42:1836–1849.

Minet, J., S. Lambot, E. Slob, and M. Vanclooster. 2010. Soil surface water content estimation by full-waveform GPR signal inversion in the presence of thin layers. IEEE Trans. Geosci. Remote Sensing 48:1138–1150.

Moghadas, D., F. André, H. Vereecken, and S. Lambot. 2010. Efficient loop antenna modeling for zero-offset, off-ground electromagnetic induction in multilayered media. Geophysics 75(4), doi:10.1190/1.3467936.

Noborio, K. 2001. Measurement of soil water content and electrical conductivity by time domain reflectometry: A review. Comput. Electron. Agric. 31:213–237.

Pepin, S., N.J. Livingston, and W.R. Hook. 1995. Temperature-dependent measurement errors in time domain reflectometry determinations of soil water. Soil Sci. Soc. Am. J. 59:38–43.

Robinson, D.A., J.P. Bell, and C.H. Batchelor. 1994. Influence of iron minerals on the determination of soil-water content using dielectric techniques. J. Hydrol. 161:169–180.

Robinson, D.A., S.B. Jones, J.M. Wraith, D. Or, and S.P. Friedman. 2003. A review of advances in dielectric and electrical conductivity measurement in soils using time domain reflectometry. Vadose Zone J. 2:444–475.

Robinson, D.A., T.J. Kelleners, J.D. Cooper, C.M.K. Gardner, P. Wilson, I. Lebron, and S. Logsdon. 2005. Evaluation of a capacitance probe frequency response model accounting for bulk electrical conductivity: Comparison with TDR and network analyzer measurements. Vadose Zone J. 4:992–1003.

Schaap, M.G., D. Robinson, S. Friedman, and A. Lazar. 2003. Measurement and modeling of the TDR signal propagation through layered dielectric media. Soil Sci. Soc. Am. J. 67:1113–1121.

Shuai, X., O. Wendroth, C. Lu, and C. Ray. 2009. Reducing the complexity of inverse analysis of time domain reflectometry waveforms. Soil Sci. Soc. Am. J. 73:28–36.

Sihvola, A.H., and J.A. Kong. 1988. Effective permittivity of dielectric mixtures. IEEE Trans. Geosci. Remote Sensing 26:420–429.

Stillman, D., and G. Olhoeft. 2008. Frequency and temperature dependence in electromagnetic properties of Martian analog minerals. J. Geophys. Res. 113:E09005, doi:10.1029/2007JE002977.

Sun, Z.J., G.D. Young, R.A. McFarlane, and B.M. Chambers. 2000. The effect of soil electrical conductivity on moisture determination using time-domain reflectometry in sandy soil. Can. J. Soil Sci. 80:13–22.

Topp, G.C., J.L. Davis, and A.P. Annan. 1980. Electromagnetic determination of soil water content: Measurements in coaxial transmission lines. Water Resour. Res. 16:574–582.

Topp, G.C., J.L. Davis, and A.P. Annan. 2003. The early development of TDR for soil measurements. Vadose Zone J. 2:492–499.

van Dam, R.L., W. Schlager, M.J. Dekkers, and J.A. Huisman. 2002. Iron oxides as a cause of GPR reflections. Geophysics 67:536–545.

Weerts, A.H., J.A. Huisman, and W. Bouten. 2001. Information content of time domain reflectometry waveforms. Water Resour. Res. 37:1291–1299.

West, L.J., K. Handley, Y. Huang, and M. Pokar. 2003. Radar frequency dielectric dispersion in sandstone: Implications for determination of moisture and clay content. Water Resour. Res. 39:1026.

Yu, C., A.W. Warrick, and M.H. Conklin. 1999. Derived functions of time domain reflectometry for soil moisture measurement. Water Resour. Res. 35:1789–1796.

Zhou, C., L. Liu, and J.W. Lane. 2001. Nonlinear inversion of borehole-radar tomography data to reconstruct velocity and attenuation distribution in earth materials. J. Appl. Geophys. 47:271–284.